Rapid Urban Roadside Tree Inventory Using a Mobile Laser Scanning System

Yiping Chen, *Member, IEEE*, Shiqian Wang, Jonathan Li, *Senior Member, IEEE*, Lingfei Ma, *Student Member, IEEE*, Rongren Wu, Zhipeng Luo, *Student Member, IEEE*, and Cheng Wang, *Senior Member, IEEE*

***Abstract*—This paper presents a feasible workflow for use of three-dimensional point clouds acquired by a vehicle-borne mobile laser scanning (MLS) system for urban tree inventory. Extracting geometrical information, such as crown diameter, diameter at breast height (DBH), and tree height, from the MLS point clouds is a challenging task due to huge data volume, occlusions, mixed density, and irregular distribution of points in complex urban environments. The proposed workflow consists of three parts: individual tree cluster extraction, geometric parameter estimation, and tree species classification. The results show that over 93% of the roadside trees were correctly detected with an average error of about 5% in the DBH estimation when compared to field surveys and 78% of the overall accuracy was achieved for the classification of tree species.**

***Index Terms*—Mobile laser scanning, point cloud, roadside tree, tree inventory, tree species classification.**

I. Introduction

In 2050, around 66% of the world's population is expected to live in cities [1]. Rapid urbanization may result in many urban environmental problems such as poor air quality, dust, noise, and urban floods [2]. One of the possible solutions to these issues is the roadside tree, which provides superiorities including prevention of water loss and soil erosion, reduction of air pollution and road noise, and adjustment of temperature and moisture [3]. Meanwhile, roadside trees also cause problems. For example, falling tree branches may harm pedestrians, pests like the emerald ash borer can cause widespread mortality of ash trees, and allergies may occur in urban areas because of trees' pollen and seeds [4]. Thus, knowing the geometrical information and tree species of urban trees is relevant to urban tree protection, urban planning, environmental impact assessment, biomass calculation, and tree risks management. Moreover, information of tree species may help reduce damage by tree crashes because frangible (i.e., breakable) roadside trees can be planted at places that are more prone to run-off-road accidents [5].

However, urban tree inventories in many cities are often incomplete and inaccurate due to budget problems.

Based on a survey conducted in 1980, of the 2861 cities in the United States, only 511 cities had information on urban tree inventories [6]. Although most of the urban forest data in the U.S. can be found on the Internet, it is mostly derived from air photos and radar images instead of field surveys. In Canada, only 20% of municipalities have management plans for urban forests, and 25% of municipalities do not have urban tree inventories [7]. In China, many of the cities lack the funding and strategies for planning and management of urban forests [8].

Field surveys can get most of the information required for an urban tree inventory, such as species, height, diameter at the breast height (DBH) measured at 1.3 m above the ground, crown spread, soil conditions, tree condition, and location of roadside trees. However, field measurements of the DBH, tree height, and crown spread are often complicated due to accessibility problems, variations within each measurement, and confusions when dealing with different trees in different environments [9].

Besides, the traditional methods for the urban tree inventory have met plenty of challenges. Calipers and tapes have been used in studies to measure the DBH [10]. However, the accuracy of the caliper method needs to be enhanced by averaging two or more measurements at different angles [9]. Also, the accuracy of the tape method can be affected by the tilt of trees. Tree height, as another important measurement, is often calculated based on angle and distance measurements. Additionally, it is difficult to accurately measure the crown spread because the outline of tree crowns cannot be well defined. Consequently, errors are often caused by manually defined tree outlines, blocking of sight, and by estimating the crown spread based on a few measurements of radius [9]. Other methods such as aerial photointerpretation, stereo photogrammetry [11], satellite image analysis [12], synthetic aperture radar imaging [13], and Open Tree Map [14]

Manuscript received April 6, 2018; revised March 7, 2019 and June 24, 2019; accepted July 14, 2019. This work was supported in part by the National Natural Science Foundation of China under Grants 41871380 and 61601392. *(Corresponding author: Jonathan Li.)*

Y. Chen, R. Wu, Z. Luo, and C. Wang are with the Fujian Key Lab of Sensing and Computing for Smart Cities, School of Informatics, Xiamen University, Xiamen 361005, China (e-mail: chenyiping@xmu.edu.cn; wrremail@stu.xmu.edu.cn; zpluo@stu.xmu.edu.cn; cwang@xmu.edu.cn).

S. Wang was with the Department of Geography and Environmental Management, University of Waterloo, Waterloo ON N2L 3G1, Canada. She is now with the Department of Geography, Florida State University, Tallahassee, FL 32306-1400 USA (e-mail: sw18d@my.fsu.edu).

J. Li is with the Fujian Key Lab of Sensing and Computing for Smart Cities, School of Informatics, Xiamen University, Xiamen 361005, China, and also with the Department of Geography and Environmental Management, University of Waterloo, Waterloo ON N2L 3G1, Canada (e-mail: junli@xmu.edu.cn).

L. Ma is with the Department of Geography and Environmental Management, University of Waterloo, Waterloo ON N2L 3G1, Canada (e-mail: l53ma@uwaterloo.ca).

Color versions of one or more of the figures in this paper are available online at http://ieeexplore.ieee.org.

Digital Object Identifier 10.1109/JSTARS.2019.2929546

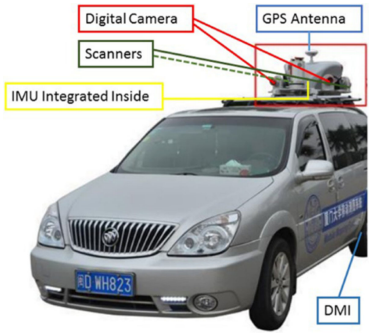

Fig. 1. Components of a typical MLS system.

also have their limitations including the limited resolution of the imagery, affection of weather conditions, and difficulties for georegistration.

With the fast development of light detection and ranging technology, tree classification and feature extraction have entered a new era. Airborne laser scanning (ALS) systems, with their large coverage and top view of forests, have been widely used for many forestry applications such as canopy mapping, biomass estimation, and tree species classification [15], [16]. However, the point density of the ALS systems is only about 25 points/m² at 400-m flying height [16]. Terrestrial laser scanning (TLS) can obtain higher point density and can be placed in high-density forests where vehicles cannot reach. However, occlusion problems and the difficulties of moving the platform can lower the efficiency and feasibility of data collection [17].

Compared with the ALS, mobile laser scanning (MLS) data are used less in urban tree inventory due to some of its limitations: smaller coverage, larger data volume, and higher cost. However, an MLS has a side view that can directly scan tree trunks, which cannot be seen in ALS data. Also, the point density of the MLS used in this study is more than 3000 points/m^2 near trajectory and 300 points/m^2 for tree points. Thus, MLS provides the potential for simultaneous and automated extraction of the roadside tree information. This can be achieved through road surveys to help update current roadside tree inventories.

Fig. 1 shows the components of an MLS system. An MLS system is an integrated platform consisting of four parts: one mobile platform; one or more laser scanners; a high-precision positional system; and one or more digital cameras [18].

The mobile platform carries the laser scanners and other components [18]. The control system is often located in the front seat where people can adjust the scan mode and observe data output. The positional information of an MLS platform and an inertial measurement unit (IMU) is often updated by the global navigation satellite system (GNSS) [19]. At places where the GNSS signal is deteriorated by high-rise buildings and tunnels, the IMU and a distance measuring indicator (DMI) units can observe the moving distance, acceleration, roll, pitch, and heading of the vehicle to update the positioning information [19]. Also, digital cameras are often mounted on the top of the vehicle to take videos or color images of the surveyed area simultaneously, while three-dimensional (3-D) point clouds are collected by the laser scanners.

TABLE I
DATASETS USED IN THIS STUDY

Dataset	A	B	C	D
Tree types	2	1	7	NA
Tree density	Scattered	Closely arranged	Scattered	Closely arranged
Time	2013/11/25	2017/8/20	2015/9/12	2013/8/21
Road width (m)	25	30	35	25
Road length (m)	9047	525000	9000	500
Scan type	One-way	One-way	One-way	Two-way
Point density (pts/m^2)	4000	1000	1000	8000
Vehicle speed (km/h)	50	50	50	25
Number of samples	980	113000	970	54
Number of training samples	780	100000	765	44
Number of testing samples	200	13000	205	10
Location	Biberach street, Germany	Area outside xiamen island	Huandao Road, Xiamen	Kingston, Ontario

II. STUDY AREA AND DATA

In this study, a total of four datasets were collected and used, in which the Datasets A acquired by Trimble MX9 is located in Biberach street, Germany, and B and C are located in the city of Xiamen, Fujian, China, where the roadside trees are dense and contain a lot of tropical plants. The crowns of these tropical plants are smaller and the wide variety of roadside trees in the datasets can be used to test the classification algorithms. The Dataset D was collected in the city of Kingston, ON, Canada, where many conifer trees grow in a variety of heights and sizes (see Table I).

Two Datasets B–C were collected by a RIEGL VMX-450 system from Xiamen University in Xiamen, and the Dataset D was provided by Tulloch Engineering, also using a RIEGL VMX-450 system.

The Dataset C is the simplest one with only two types of trees planted at wide intervals. However, a great number of cars, pedestrians, light poles, road signs, and bus stops in the Dataset C caused occlusions of tree trunks. Trees in the Dataset B [42] were planted close to each other with high grasses and shrubs near the tree trunks, making the segmentation of individual trees challenging. These two datasets were used for geometrical information extraction. The Dataset C, with seven different kinds of tree species, was used for both geometrical information extraction and testing of classification methods. The Dataset D is characterized by the high point density and large conifer trees near the road.

III. METHOD

A. Proposed Workflow

During the process of single tree extraction, three different methods were tested and compared: Euclidean clustering; Ncut; and region growing segmentation. After the tree clusters were

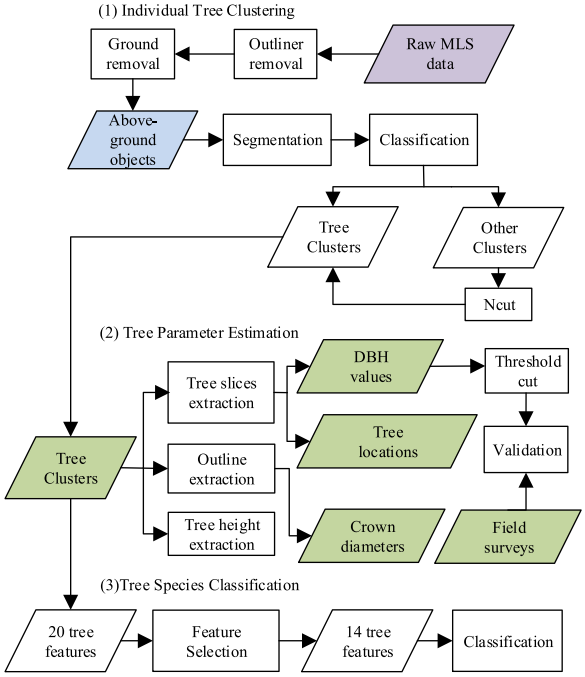

Fig. 2. Three steps of our workflow: (1) individual tree clustering, (2) tree parameter estimation, and (3) tree species classification.

extracted, a two-dimensional (2-D) alpha shape method was used to obtain cluster outlines. As shown in Fig. 2, the entire workflow can be divided into four parts: extraction of single trees; tree parameters estimation; tree species classification; and validation.

During the process of single tree extraction, four different methods were tested and compared: Euclidean clustering [26]; Ncut [28]; region growing segmentation [27]; and supervoxel-based segmentation [29]. After the tree clusters were extracted, a 2-D alpha shape method [41] was used to obtain cluster outlines. The random sample consensus (RANSAC) fitting method and a bounding rectangle method were used for calculating the DBH. Then, the parameters such as tree height, total point number, point density, and point number for each height percentile, and standard deviation (SD) of the point height were applied to the classification method. After using the recursive feature elimination (RFE) method to select relevant features, two different classifiers, k-nearest neighbor (k-NN) [32] and random forests (RF) [33] were applied. In this study, Datasets C and D were chosen since they have more tree species. Finally, the estimations of the DBH and tree species classification results were validated.

B. Individual Tree Clustering

Since MLS data cannot accurately capture objects that are far from the scanning trajectory, the redundant data that are far from the trajectory were removed. Then, a statistical outlier removal filter was used to remove outliers (noise points that are not GNSS or IMU errors and multipath reflections) [20]. Outliers can cause problems during data processing because these points can lead

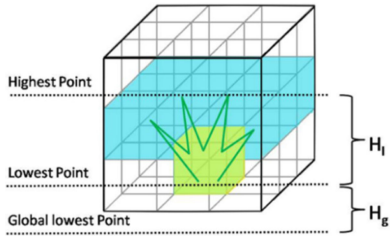

Fig. 3. Upward growing for ground removal.

to erroneous changes in surface normal, point coordinates, and curvatures.

The statistical outlier removal filter computes distances of all points using k-NN. Then, the global mean distance and standard deviations of the distances are calculated. Points with a mean distance to their k-NN that exceeds the interval defined by the global mean and standard deviation are removed from the data. The default setting of the threshold is

$$d_{\max} = d_a + n * \mathrm{sd} \tag{1}$$

where $d_{\max}$ is the threshold, d_a is the average distance, sd is the standard deviation of the average distance, and n is the multiplier. Different n values were tested and it was set as 10 to make sure no tree points were removed.

Also, a large proportion of MLS points are ground points, their removal can improve the processing speed and facilitate later processes. Ground removal has been well studied by researchers to facilitate forestry analysis, hydrology analysis, and geological hazard control [21]. Most of the ground-filtering algorithms are based on slope, interpolation, morphological filters, and hybrid methods [22]. However, raster-based methods can lower the accuracy of derived ground points, and interpolation-based methods may not work for MLS data due to the large data volume. Thus, the upward growing method was employed in this study to enhance the efficiency and accuracy of the segmentation.

Fig. 3 shows a simple example of the upward growing approach to ground removal. First, the point clouds were voxelized. Second, the green voxel in Fig. 3 is selected as a seed voxel, and the blue voxels are the nine upward voxels searched. The height difference between the lowest point in the bottom voxel and the highest point in the top voxel is defined as H_l. The height difference between the lowest point in the bottom voxel and the lowest point in the data scene is defined as H_g. Finally, if the H_l is smaller than the local terrain relief and H_g is smaller than the global terrain relief, the voxel clusters are classified as ground points [23].

Many segmentation methods were developed for single tree extraction. Some methods required the rasterizing of point cloud data may cause problems such as mixed pixels, interpolation, and empty pixels, which will reduce the data accuracy. Additionally, small trees that grow under big trees or grow near big trees are often neglected in these methods. [24].

Some studies combine multispectral data with ALS data to identify individual trees after tree tops were found using a crown

height model [25]. However, registration of different data types will involve geo-correction processes and may produce errors.

Finally, four different segmentation methods were tested for extraction of single tree clusters: Euclidean distance clustering [26]; region growing segmentation [27]; normalized cut [28]; and supervoxel-based segmentation [29].

1) Euclidean Distance Clustering: The method can cluster points based on the points' Euclidean distances to its neighbors according to a user-defined distance threshold. However, setting the threshold for the method is difficult because a small distance threshold may lose tree points and a large threshold cannot segment close objects. To define the appropriate distance threshold, the average distance between adjacent points needs to be manually observed. The optimal distance threshold was found by adjusting different values around the average distance.

2) Region Growing Segmentation: First, the curvatures of all points in the Dataset are calculated using the nearest neighbors around each point. Points with the lowest curvatures are selected as seed points. Second, the angle differences between the seed points and their neighbor points are calculated. When the difference is smaller than the angle threshold set by the user, the points are added to the cluster. Third, the neighbor points that have smaller curvatures than the defined curvature threshold are added to the seed list, and the original seeds are removed. The algorithm will restart the search when the seed set is empty.

3) Normalized Cut (Ncut): First, the MLS data were divided into voxels. Second, the nonempty voxels were selected and the similarities among each pair of voxels were computed by [26]

$$w_{ij} = \begin{cases} \exp\left(-\frac{\left\| p_i^{XY} - p_j^{XY} \right\|_2^2}{\sigma_{XY}^2} \right) * \\ \exp\left(-\frac{\left| p_i^{Z} - p_j^{Z} \right|^2}{\sigma_{Z}^2} \right), \text{ if } \left\| p_i^{XY} - p_j^{XY} \right\|_2 < d_{XY} \\ 0, \quad \text{otherwise} \end{cases} \tag{2}$$

where $p_i = (x_i,\, y_i,\, z_i)$ and $p_j = (x_j,\, y_j,\, z_j)$ are the centroids of voxels *i* and *j*. $p_i^{XY} = (x_i,\, y_i)$ and $p_j^{XY} j = (x_j, y_j)$ are the coordinates of the centroids on the *X–Y* plane, and $p_i^Z = z_i$ and $p_j^Z = z_j$ are the z coordinates of the centroids. σ_{xy} and σ_Z are the standard deviations. d_{XY} is the maximum threshold of the horizontal distance between two voxels. The centroid of voxel *i* is defined as follows:

$$p_i = \frac{1}{N_i} \sum_{m=1}^{N_i} p_m^i \tag{3}$$

where N_i is the total number of points within voxel *i* and p_m^i is a point within voxel *i*.

Third, the method divided the point clouds into groups by maximizing the similarities in each group and minimizing similarities between different groups using the following equation:

$$\mathrm{Ncut}\,(A, B) = \frac{\mathrm{cut}\,(A, B)}{\mathrm{assoc}\,(A, V)} + \frac{\mathrm{cut}\,(A, B)}{\mathrm{assoc}\,(B, V)} \tag{4}$$

where $\mathrm{cut}(A, B)$ is the total sum of weights between voxel groups *A* and *B*, and $\mathrm{assoc}(A, V)$ is the sum of the weights of all edges ending in the voxel group *A*.

The minimized *Ncut(A,B)* is derived by solving the generalized eigenvalue problem (Shi and Malik, 2000)

$$(D - W)\, y = \lambda D y \tag{5}$$

where *D* is a diagonal matrix with $D(i,\ i) = \sum_m w_{im}$.

4) Supervoxel-Based Segmentation: A voxel can be transformed into a supervoxel by assigning properties such as the geometrical center of the voxel, mean laser reflectance intensity value of constituting 3-D points, and surface normal [28]. After the supervoxels were extracted, they were projected to the *X–Y* plan and a convex hull was used to represent their area. Information such as the highest point, lowest point, bounding box, and the gravity center of the super voxels was also extracted. The coordinates of the gravity center were calculated by

$$\begin{aligned} x &= \frac{\sum_{i=1}^{n} x_{pi}}{n} \\ y &= \frac{\sum_{i=1}^{n} y_{pi}}{n} \end{aligned} \tag{6}$$

where p_i belongs to the supervoxel, and *n* is the number of points in the supervoxel.

Supervoxels near the local highest points were considered trunk voxels. Then, trunk voxels that have the highest point below a user-defined threshold were removed. This threshold should be higher than the average bush height of the area. Finally, the complete tree cluster was derived by growing both upward and downward [30].

C. Tree Species Classification

First, 100, 95, 85, 70, 55, 40, and 25th percentile in height were selected to cut the tree clusters into horizontal slices. We chose the percentage because that 95% and 70% of trees are mostly crowns, and between 70% and 25% are mainly DBH, and 0% $\sim$ 25% includes weeds. For each slice, two parameters were calculated: the point density and point number.

Second, the RFE method was applied to enhance the classification accuracy because some of the features of the tree clusters may produce noise. The goal of RFE was to select features by recursively considering smaller and smaller sets of features [31].

Finally, two different classification methods were tested: the k-NN [32] and the Random forests (RF) [33].

D. Estimation of Tree Parameters

1) Diameter at Breast Height (DBH): Some studies use least squares adjustment to estimate the DBH using field survey data and features such as tree height, crown area, crown volume, and crown height [26]. Some other studies use cylinder model fitting and cone fitting methods to estimate the DBH [17]. Based on a former study, the cone fitting method achieved best results when the tree trunks were used in the fitting; the two methods worked considerably the same when using trunk slices [34]. In this study, the cylinder fit method for trunk slices and the circle fit method for projected points of slices were applied to estimate the DBH. First, a threshold cut method was used to cut the tree clusters to extract tree trunks.

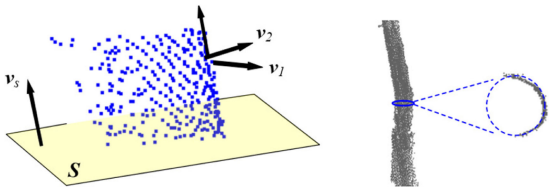

Fig. 4. Plane perpendicular to trunk and circle fit.

Fig. 5. Extracted stems.

In the cylinder fit method, the RANSAC cylinder detection method was applied to determine the location of the tree center and estimate the DBH from the trunk slices, the RANSAC cylinder detection method was applied [35]. While in the circle fit method, the slice points were first projected onto a plane perpendicular to the trunk direction and then rotated to the XY plane for circle fitting. The normal vector of the plane perpendicular to trunk was estimated by the following formula:

$$\boldsymbol{v}_s = \mathrm{Nor}\left(\sum_{i=1}^{M}\sum_{j=1}^{M}(\boldsymbol{v}_i \times \boldsymbol{v}_j)\cdot \mathrm{sgn}(Z_{ij})\right) \tag{7}$$

where M is the number of points in the point clouds, v_i is the normal vector of point i. $\mathrm{sgn}()$ is the sign function, Z_{ij} is the Z component of $\boldsymbol{v}_i \times \boldsymbol{v}_j$ and $\mathrm{Nor}(\boldsymbol{v})$ represents the normalizing vector $\boldsymbol{v}$. Suppose the normal vector of this plane v_s is (A, B, C), then the projected point p_i can be rotated to the XY plane by the left-multiple rotation matrix $\mathcal{R}$.

$$p_i' = \mathcal{R}p_i \tag{8}$$

where the rotation matrix $\mathcal{R}$ can be

$$\mathcal{R} = \begin{bmatrix} A & B & C \\ \frac{B}{B-A} & \frac{-A}{B-A} & 0 \\ -\frac{AC}{B-A} & \frac{BC}{B-A} & B+A \end{bmatrix}. \tag{9}$$

There may be some noise points around the trunk, so the RANSAC algorithm with the circle model was used to filter these noise points. After filtering, a circle fitting method is used on projected points to acquire the location and DBH of tree trunk. Fig. 4 illustrates the detail of the circle fit method.

Estimation of the DBH for noncircular trunks using this method can be problematic [40]. Thus, the two methods were compared with a proposed minimum bounding rectangle method in this study. This minimum bounding rectangle method uses the width of the minimum bounding box of each trunk cluster to estimate the DBH. Fig. 5 shows the results using our method. It can be seen that our method achieved good performance.

2) Tree Height: There are two approaches to extract tree height using point clouds. One method uses the height difference between highest tree points and the height of digital terrain model (DTM) to represent the height of trees [16]. However, errors in DTM will influence this estimation. Another method uses the height difference between the highest tree points and the lowest tree points to estimate tree heights [17]. To enhance the efficiency of the algorithm, DTM of the study area was not generated and the single tree cluster-based height estimation method was applied.

Studies have revealed that although the point density of the TLS is very high, the laser beam cannot penetrate tree leaves and reach tree tops, causing underestimations of tree heights [17]. Also, the underestimation of tree heights can be caused by occlusion at lower parts of tree trunks, bushes, and grass.

3) Crown Spread: Crown spread estimation is important for off-ground biomass estimation. 78% of the biomass variance can be explained by crown diameter alone and the crown diameter can enhance the accuracy of the estimation of biomass for 0.24 in R^2 and 7 t/ha in root mean square error (RMSE) [36]. The estimation accuracy of the crown diameter can be affected by stand density [37]. This difficulty was also found during the processing of MLS point clouds due to the segmentation problem of dense vegetation. In this study, a 2-D alpha shape outline extraction method was used to extract the outline of each tree clusters [38], [39]. Then, the RANSAC shape detection method was used to extract the crown diameter for trees with a rounded crown. Crown spread is derived by the spoke method for trees with irregular crown shapes. The spoke method calculates the average distance from outline points to the trunk center to represent the crown diameter.

IV. Results and Discussion

A. Tree Extraction

First, buildings and other objects far from the trajectory can be removed based on the point distance to the scan line.

Outlier points of the datasets were found in the air, below ground surface, and near object surfaces. The number of nearest points was set as 30 and the SD multiplier was set as 5 for the statistical outlier removal filter. The processing speed of the algorithm was about 30 s for a 100-MB scene and the method can remove most of the outliers far from objects. However, it cannot filter clustered outliers so these points need to be removed manually.

The upward growing ground filtering method has certain limitations when applied in scenes with high ground level differences because the global relief set by the user may affect the filtering results. For example, Fig. 6 shows that the higher road points were not extracted when using a 2-m global relief threshold. This can be alleviated by dividing the road into smaller scenes or changing the global relief threshold to a larger value.

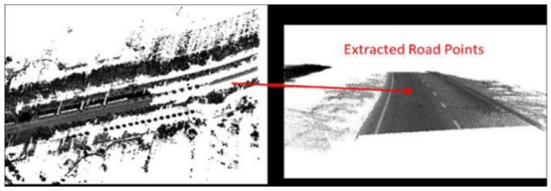

Fig. 6. Ground point removal using a 2-m global relief threshold.

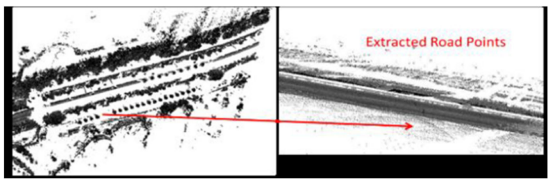

Fig. 7. Ground points removal using a 10-m global relief.

Fig. 8. Results of the Euclidean distance clustering. (a) 0.1-m distance threshold. (b) 0.3-m distance threshold.

Fig. 9. Segmentation results of the region growing using (a) number of neighbor = 20, and (b) number of neighbor = 10.

Fig. 7 shows the result when the global relief was set as 10 m. However, this can lower the time efficiency of the algorithm by around 10 s, and some of the points and small clusters were filtered as ground points as shown in the right side of Fig. 7. These error points may affect the generation of DTM. However, their impact on tree species classification and tree extraction can be small.

Results of the Euclidean distance method are shown in Fig. 8. A large threshold will merge the connected trees; a smaller threshold may separate the connected trees but some trees can be clustered into different parts.

It can be seen by comparing Figs. 8(b) and 9(a) that some of the tree trunks were separated from the tree crowns when the search number of their neighbors was set smaller by region growing. In the region growing algorithm, the smaller the number of neighbors is, the more accurate the segmentation of its single tree is. Each color represents the classification of trees coarse clustering, and each cluster is distinguished by different colors. The number of neighbor in Fig. 9(a) was set as 20, the segmentation accuracy rate is only 57.1%, and the green parts are connected because they are too close. The number of neighbor in Fig. 9(b) was set to 10 and a better segmentation result was obtained. The clusters are distinguished by different colors, except the left part where three and four trees are combined.

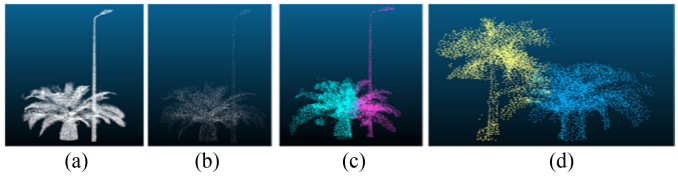

Fig. 10. Results of Ncut segmentation obtained: (a) via Euclidean distance clustering, (b) from downscaled high-density point cloud, (c) tree connected with a light pole, and (d) two connected trees.

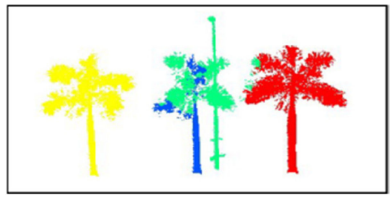

Fig. 11. Results of trees connected with a light pole obtained via supervoxel-based segmentation.

The MLS data have high point densities that require high memory space when processed using the Ncut method.

Thus, the original dataset, as shown in Fig. 10(a), was subsampled to the cloud shown in Fig. 10(b). The point number decreased from 36 901 to 5367 to enable the data to be processed using the Ncut method. As can be seen from Fig. 10(c), the segmentation can separate electricity poles from the trees. Fig. 10(d) shows that the method can also segment the connected trees.

Although the clusters with more than one tree can easily be classified and be segmented using the Ncut method, the loss of tree points may cause errors in the geometrical measurement of the tree. A better result could be obtained using the Ncut method if a more powerful computer would be used.

Fig. 11 shows the results of tree extraction and segmentation from the Dataset C using the supervoxel-based method. It can be seen that higher trees are accurately located.

The advantage of the supervoxel-based method is that it can separate some connected objects as shown in Fig. 10. However, some smaller trees and closely clustered trees were not detected. The method also worked poorly for the Dataset B due to tilted tree trunks and branching. The advantage of the supervoxel-based method is that it can segment trees connected to light poles and traffic signs. However, smaller trees were not detected during the segmentation.

Fig. 12 shows the results of tree extraction from the Dataset A using the supervoxel-based method.

Fig. 13 shows some errors found in the results of segmentation (detected trees are shown in red): small trees that were excluded due to low point number in their clusters, errors caused by light poles or traffic signs, unconnected tree parts, errors caused by closely connected trees and bushes, and occlusion caused by bushes.

Fig. 12. Results of roadside trees extraction.

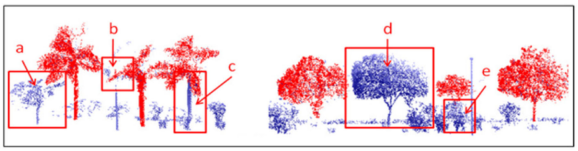

Fig. 13. Errors and undetected trees.

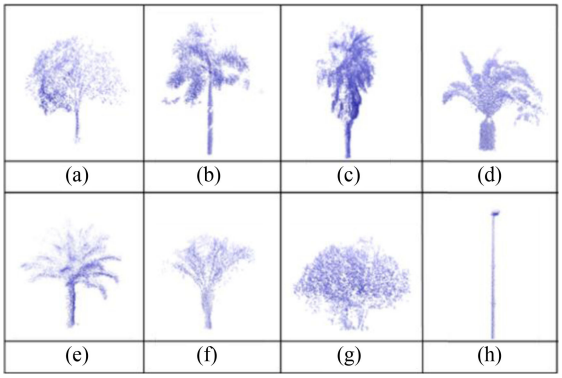

Fig. 14. Selected classes. (a) *Bischofia polycar.* (b) *Roystonea regia.* (c) *Washingtonia filifera.* (d) *Sago cycas.* (e) *Sylvester palm.* (f) *Triangle palm.* (g) Bushes. (h) Light pole.

To conclude, the results of the Euclidean distance segmentation were adopted for the following methods due to its high efficiency. The undetected tree rates of the method for Datasets A, B, and C were 4.7%, 10.7%, and 2.7%, respectively.

The lowest detection rate was obtained from the Dataset B because some of the trees were planted in two rows causing occlusion. The segmentation result was more accurate for the Dataset C, which may indicate that segmentation of trees with similar sizes and species is easier than segmentation of trees with different sizes and species.

B. Feature Selection

First, the single tree clusters were manually labeled as different classes as shown in Fig. 14.

Second, the clusters were cut into different horizontal slices based on height percentiles.

At last, Top 14 features with high importance were extracted based on the RFE method: height, *x*-width, *y*-width, SD, density 40–55%, density 55–70%, density 70–85%, density 85–95%, density 95–100%, point number 0–25%, point number 25–40%, point number 40–55%, point number 85–95%, and point number 95–100%.

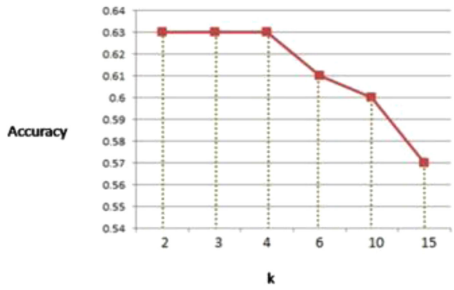

Fig. 15. Accuracies obtained using different *k* values.

TABLE II
CONFUSION MATRIX OF k-NN CLASSIFICATION

	a	b	c	d	e	f	g	h	Total	Recall
a	8	5	0	0	1	0	1	0	15	0.53
b	0	56	31	13	1	3	0	0	104	0.54
c	0	2	30	0	0	0	0	0	32	0.94
d	1	0	0	15	2	4	0	0	22	0.68
e	3	0	0	2	4	1	0	0	10	0.40
f	0	0	0	0	0	6	0	0	6	1
g	2	0	0	1	0	1	2	0	6	0.33
h	0	1	0	0	0	0	0	9	10	0.90
Total	14	64	61	31	8	15	3	9	205	
Precision	0.57	0.88	0.49	0.48	0.50	0.40	0.67	1	OA = 63%	

TABLE III
CONFUSION MATRIX OF RANDOM FOREST CLASSIFICATION

	a	b	c	d	e	f	g	h	Total	Recall
a	8	5	0	0	1	0	1	0	15	0.53
b	0	83	17	1	1	2	0	0	104	0.80
c	1	2	28	1	0	0	0	0	32	0.88
d	0	2	0	17	0	3	0	0	22	0.77
e	0	1	0	1	4	2	2	0	10	0.40
f	0	0	0	0	0	6	0	0	6	1
g	0	0	0	0	0	2	4	0	6	0.67
h	0	0	0	0	0	0	0	10	10	1
Total	9	93	45	20	6	15	7	10	205	
Precision	0.89	0.89	0.62	0.85	0.67	0.4	0.57	1	OA = 78.1%	

C. Classification

As shown in Fig. 15, the method achieved the highest accuracy when selecting the *k* values as 2, 3, and 4, respectively.

Table II and Table III show the confusion matrix of the classification using the k-NN method and random forest, respectively. The result shows that around 30% of *Roystonea Regia* were classified as *Washingtonia Filifera* because the two-tree species share similar geometrical shapes, the light poles can be easily

TABLE IV
OVERALL ACCURACY AND RMSE FOR DBH ESTIMATION USING MINIMUM BOUNDING RECTANGLE METHOD

Dataset	Average DBH Estimated (cm)	Average DBH Reference (cm)	Overall Accuracy (%)	RMSE (cm)
A	29.0	32.1	90.2	6.6
B	33.1	33.9	97.5	4.9
C	41.2	44.5	92.6	7.3
All	34.8	36.8	94.6	5.0

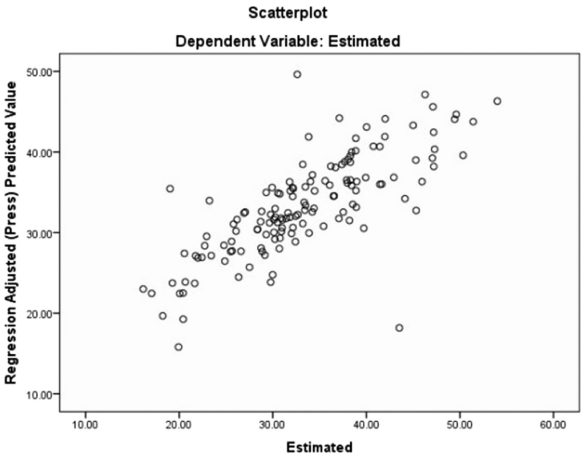

Fig. 16. Linear regression of DBH using all data inputs (cm).

separated from trees, smaller trees such as *Bischofia Polycar*, *Sylvester palm, triangle palm*, and bushes are more difficult to classify.

D. Estimation of Tree Parameters

Table IV lists the results of the DBH estimation. Due to occlusion in some datasets, 151 of 163 trees surveyed were included in accuracy assessment. The minimum bounding rectangle method tends to underestimate the DBH values because the MLS data used in this study cannot capture more than half of the tree trunks all the time. The Dataset C received the lowest overall accuracy (OA) in the tree datasets because the data are noisier than the other two datasets. The OA of the Dataset C is lower than that of the Dataset B because the tree trunks in the Dataset C are not as symmetrical as trunks in the Dataset B. Also, the field survey data for the Dataset C may be less accurate than that of the Dataset B for the following three reasons.

1) Some of the trees in the Dataset C have rough bark that may cause inaccurate perimeter measurements.
2) The ground in the Dataset C is uneven and has very soft soil on the surface, which may cause inaccurate height measurements.
3) Some of the trees in the Dataset C start to branch at 1 m height, which leads to enormous DBH changes around the trunk slice in the area.

The result of linear regression result of the DBH estimation is shown in Fig. 16. The R^2 is 0.602 and the standard error of the estimation is 5.0 cm. The linear regression parameters are shown by

$$D = 0.734d + 6.788 \tag{10}$$

TABLE V
REGRESSION RESULTS USING BOUNDING RECTANGLE METHOD AND CYLINDER FIT METHOD

Dataset	Method	R^2	Standard error (cm)
A	Bounding Rectangle	0.422	3.9
B		0.426	5.7
C	Cylinder fit	0.765	4.0
All		0.025	8.8

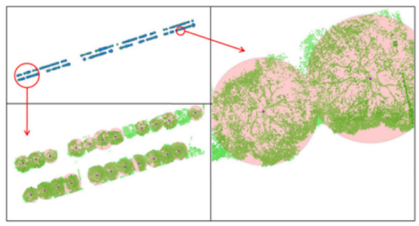

Fig. 17. Results of crown diameter estimation.

where d is the derived DBH and D is the regression-adjusted DBH.

Table V shows the R^2 and standard error of estimation for the three datasets and the result of the cylinder fit for the Dataset C. For 53 trees in the Dataset C, 9 of the trunk slices failed to fit the RANSAC cylinder detection method. Ten of the 44 derived DBH results had a higher error than 2 times RMSE. R^2 of the cylinder fit method is also very small and the standard error is much higher than that of the bounding rectangle method. The Dataset C achieved the highest R^2 among the three datasets; however, the standard error of the Dataset A is nearly the same as the Dataset B.

Fig. 17 shows the result of the crown diameter estimation of the Dataset B overlaid with the original point clouds. The proposed method can estimate crown diameter when trees are connected and deal with missing data. Also, the tree trunks were successfully located within true trunk boundaries using the center of the minimum bounding boxes. However, the electrical poles and road signs caused errors in estimation.

V. CONCLUDING REMARKS

The results of this study show that the MLS can assist urban roadside tree inventory to achieve higher time efficiency, tree species classification accuracy, and DBH estimation accuracy, compared with the ALS. However, there are several unsolved problems. Since raw MLS data are often very large, the dataset must be divided into smaller files to be processed. The result of such processes may lead to objects near the separation line being divided into parts, which may cause errors in later processes. The removal of outlier points in the MLS data can be crucial for ground filters. However, setting a smaller threshold may result in tree points classified as outliers. Also, clustered outliers can be difficult to remove using the statistical outlier removal method. Ground point removal can enhance the segmentation accuracy and efficiency. However, the removal of the ground point can

be difficult for the MLS data due to the large data volume. The voxel-based upward growing algorithm can remove the ground points with high accuracy and efficiency.

There were four segmentation methods compared in this study. The Euclidean distance clustering is simple to use but cannot correctly separate closely connected trees. The Ncut method obtains the best segmentation result and separates closely connected trees. However, the method needs users to observe the number of clusters that need to be segmented and requires too much memory space. The supervoxel-based segmentation can segment connected trees but it may cause missing points during the process. To obtain better segmentation results and better efficiency, the Ncut method can be applied after the Euclidean distance clustering.

The OA of tree species classification is around 78%, which is better than using the ALS, but lower than the deep learning method presented in [19], which was 80%. The waveform transform of horizontal slices attribute in their study seems better at representing the shape of trees. The classification accuracy increased after using an RFE feature selection method because of a large numbers of feature types and the noise in the input data. Also, the RF classifier achieved better classification accuracy than the k-NN.

Although the RANSAC cylinder fit method can be more accurate than the bounding rectangle method, it may not work for irregular tree trunks. The circle fit method can be used to represent round crowns, but the 2-D alpha shape method can be used to estimate tree crowns with different shapes. The overall accuracy of the DBH estimation using the bounding rectangle method is around 95%.

The occlusions at the bottom of tree trunks may result in errors in the height estimation. Thus, future studies may use the ground height near the trunk to calculate the tree height. The occlusions at the trunk slices may result in errors in the DBH estimation. Thus, future studies may cut more than one horizontal slice to estimate the DBH.

Occlusions can also cause problems for the DBH estimation for conifer trees because the tree trunks are often occluded by brunches. The extraction of such trunks can be difficult using only segmentation methods. However, the intensity value may be helpful to separate trunk points from leaf points. To reduce occlusions, data collection from two directions or two sides of trees can achieve better data for the DBH estimation.

The high point density of the MLS data can cause the following three problems.

1) The data have to be cut into small pieces that may cut trees into two parts.
2) Some parts of tree points may be removed when the threshold cut method is used to remove points that are far from the trajectory.
3) The processing time for the datasets can be very long.

Uneven point density in the MLS data can also cause problems for segmentation algorithms based on distances between nearest points. Thus, the user-defined thresholds may not work for trees far from the trajectory. Also, trees with a wide crown spread can be segmented into two parts because the point density varies. For future studies of the high point density MLS data that have large trees in the surveyed area, the normalization or subsampling of the point cloud may be necessary.

Classification accuracy may be improved by a waveform transform of tree horizontal attributes, adding more features and samples, or using true color MLS data or multispectral MLS data. The degree of automation of the proposed method is damaged by manually setting thresholds for outlier removal and clustering methods. Some small trees were not detected since small clusters were discarded during the segmentation process. Future studies can include classification of small clusters to extract these small trees.

REFERENCES

[1] S. Roy, J. Byrne, and C. Pickering, "A systematic quantitative review of urban tree benefits, costs, and assessment methods across cities in different climatic zones," *Urban Forestry Urban Greening*, vol. 11, no. 4, pp. 351–363, 2012.

[2] M. N. Islam, K. S. Rahman, M. M. Bahar, M. A. Habib, K. Ando, and N. Hattori, "Pollution attenuation by roadside greenbelt in and around urban areas," *Urban Forestry Urban Greening*, vol. 11, no. 4, pp. 460–464, 2012.

[3] D. Armson, P. Stringer, and A. R. Ennos, "The effect of street trees and amenity grass on urban surface water runoff in Manchester, UK," *Urban Forestry Urban Greening*, vol. 12, no. 3, pp. 282–286, 2013.

[4] USDA, "Urban Tree Risk Management: A Community Guide to Program Design and Implementation," Forest Service Northeastern Area State and Private Forestry, U.S. Department of Agriculture, St. Paul, MN, USA, 1992.

[5] K. L. Wolf and N. Bratton, "Urban trees and traffic safety: Considering the US roadside policy and crash data," *J. Arboricul. Urban Forestry*, vol. 4, no. 32, pp. 170–179, 2006.

[6] J. P. Wood, "Tree inventories and GIS in urban forestry," Master's thesis, Faculty Virginia Polytechnic Inst. State Univ., Blacksburg, VA, USA, 1999.

[7] A. Bardekjian, A. Kenney, and M. Rosen, "Trends in Canada's Urban Forests," Tree, Canada: Ottawa, ON, Canada, 2016.

[8] F. Li, R. Wang, X. Liu, and X. Zhang, "Urban forest in China: Development patterns, influencing factors and research prospects," *Int. J. Sustain. Develop. World Ecol.*, vol. 12, no. 2, pp. 197–204, 2005.

[9] "American Forests Champion Trees Measuring Guidelines Handbook," American Forests, Apr. 6, 2018. [Online]. Available: http://www.americanforests.org/

[10] N. Saarinen *et al.*, "Urban-tree-attribute update using multisource single-tree inventory," *Forests*, vol. 5, no. 5, pp. 1032–1052, 2014.

[11] C. Kätsch and A. Kunneke, "Forest inventory in the digital remote sensing age," *Southern African Forestry J.*, vol. 206, no. 1, pp. 43–49, 2006.

[12] J. T. Walton, D. J. Nowak, and E. J. Greenfield, "Assessing urban forest canopy cover using airborne or satellite imagery," *J. Arboricul.*, vol. 6, pp. 334–340, 2008.

[13] F. Garestier, P. Dubois-Fernandez, I. Champion, and T. Le Toan, "Pine forest investigation using high resolution P-band Pol-InSAR data," *Remote Sens. Environ.*, vol. 115, no. 11, pp. 2897–2905, 2011.

[14] G. Morneau, "Green streets Canada urban tree inventory project," 2005. [Online]. Available: http://www.duncan.ca/pdf/Green%20Streets%20Final%20Report_11-Reduced.pdf. Accessed: Apr. 6, 2018.

[15] P. Vainio, T. Tokola, T. Palander, and A. Kangas, "A GIS-based stand management system for estimating local energy wood supplies," *Biomass Bioenergy*, vol. 33, no. 9, pp. 1278–1288, 2009.

[16] J. Reitberger, P. Krzystek, and U. Stilla, "Analysis of full waveform LiDAR data for the classification of deciduous and coniferous trees," *Int. J. Remote Sens.*, vol. 29, no. 5, pp. 1407–1431, 2008.

[17] M. Moskal and G. Zheng, "Retrieving forest inventory variables with terrestrial laser scanning TLS in urban heterogeneous forest," *Remote Sens.*, vol. 41, no. 1, pp. 1–20, 2012.

[18] I. Puente, H. González-Jorge, J. Martínez-Sánchez, and P. Arias, "Review of mobile mapping and surveying technologies," *Measurement*, vol. 46, no. 7, pp. 2127–2145, 2013.

[19] H. Guan, Y. Yu, Z. Ji, J. Li, and Q. Zhang, "Deep learning-based tree classification using mobile LiDAR data," *Remote Sens. Lett.*, vol. 6, no. 11, pp. 864–873, 2015.

[20] J. Sánchez-Lopera and J. L. Lerma, "Classification of LiDAR bare-earth points, buildings, vegetation, and small objects based on region growing and angular classifier," *Int. J. Remote Sens.*, vol. 35, no. 19, pp. 6955–6972, Oct. 2014.
[21] K. A. Razak, M. Santangelo, C. J. Van Westen, M.W. Straatsma, and S. M. de Jong, "Generating an optimal DTM from airborne laser scanning data for landslide mapping in a tropical forest environment," *Geomorphology*, vol. 190, pp. 112–125, 2013.
[22] A. S. Maguya, V. Junttila, and T. Kauranne, "Adaptive algorithm for large scale DTM interpolation from LiDAR data for forestry applications in steep forested terrain," *ISPRS J. Photogram. Remote Sens.*, vol. 85, pp. 74–83, 2013.
[23] Y. Yu, J. Li, H. Guan, and C. Wang, "Automated extraction of urban road facilities using mobile laser scanning data," *IEEE Trans. Intell. Transp. Syst.*, vol. 16, no. 4, pp. 2167–2181, Aug. 2015.
[24] W. Yao, P. Krzystek, and M. Heurich, "Tree species classification and estimation of stem volume and DBH based on single tree extraction by exploiting airborne full-waveform LiDAR data," *Remote Sens. Environ.*, vol. 123, pp. 368–380, Aug. 2012.
[25] R. Dinuls, G. Erins, A. Lorencs, I. Mednieks, and J. Sinica-Sinavskis, "Tree species identification in mixed Baltic forest using LiDAR and multispectral data," *IEEE J. Sel. Topics Appl. Earth Observ. Remote Sens.*, vol. 5, no. 2, pp. 594–603, Apr. 2012.
[26] Y. Yu, J. Li, H. Guan, C. Wang, and J. Yu, "Semi-automated extraction of street light poles from mobile LiDAR point-clouds," *IEEE Trans. Geosci. Remote Sens.*, vol. 53, no. 3, pp. 1374–1386, Mar. 2015.
[27] S. M. Abdullah, M. Awrangjeb, and G. Lu, "LiDAR segmentation using suitable seed points for 3D building extraction," *ISPRS Arch.*, vol. XL-3, no. 3, pp. 1–8, 2014.
[28] J. Shi and J. Malik, "Normalized cuts and image segmentation," *IEEE Trans. Pattern. Anal. Mach. Intell.*, vol. 22, no. 8, pp. 888–905, Aug. 2000.
[29] M. Weinmann, M. Weinmann, C. Mallet, and C. Brédif, "A classification-segmentation framework for the detection of individual trees in dense MMS point cloud data acquired in urban areas," *Remote Sens*., vol. 9, no. 3, pp. 277–305, Mar. 2017, Art. no. 277.
[30] A. K. Aijazi, P. Checchin, and L. Trassoudaine, "Segmentation based classification of 3D urban point clouds: A super-voxel based approach with evaluation," *Remote Sens*., vol. 5, no. 4, pp. 1624–1650, 2013.
[31] W. You, Z. Yang, and G. Ji, "Feature selection for high-dimensional multi-category data using PLS-based local recursive feature elimination," *Expert Syst. Appl.*, vol. 41, no. 4, pp. 1463–1475, 2014.
[32] Q. Meng, C. J. Cieszewski, M. Madden, and B. E. Borders, "K nearest neighbor method for forest inventory using remote sensing data," *GISci. Remote Sens.*, vol. 44, pp. 149–165, 2007.
[33] A. T. Hudak, N. L. Crookston, J. S. Evans, D. E. Hall, and M. J. Falkowski, "Nearest neighbor imputation of species-level, plot-scale forest structure attributes from LiDAR data," *Remote Sens. Environ.*, vol. 112, pp. 2232–2245, 2008
[34] M. McDaniel, T. Nishihata, and C. Brooks, "Terrain classification and identification of tree stems using ground-based LiDAR," *J. Field Robot.*, vol. 25, no. 6, 891–910, 2012.
[35] Y. Jin, "Matching for cylinder shape in point cloud using random sample consensus," *J. KIISE*, vol. 43, pp. 562–568, 2016.
[36] V. Kankare *et al.*, "Retrieval of forest aboveground biomass and stem volume with airborne scanning LiDAR," *Remote Sens*., vol. 5, no. 5, pp. 2257–2274, May 2013.
[37] D. Kwak *et al.*, "Estimating stem volume and biomass of Pinus Koraiensis using LiDAR data," *J. Plant Res.*, vol. 123, no. 4, pp. 421–432, 2010.
[38] H. Edelsbrunner and E. MÄucke, "Three dimensional alpha shapes," *ACM Trans. Graph.*, vol. 131, pp. 43–72, 1994.
[39] J. C. White, N. C. Coops, M. A. Wulder, M. Vastaranta, T. Hilker, and P. Tompalski, "Remote sensing technologies for enhancing forest inventories: A review," *Can. J. Remote Sens.*, vol. 42, no. 5, pp. 619–641, 2016.
[40] R. Wu, Y. Chen, C. Wang, and J. Li, "Estimation of forest trees diameter from terrestrial laser scanning point clouds based on a circle fitting method," in *Proc. IEEE Int. Geosci. Remote Sens. Symp.*, 2018, pp. 2813–2816.
[41] M. Rutainger, A. K. Pratihast, S. O. Elberink, and G. Vosselman, "Detection and modelling of 3D trees from mobile laser scanning data," *ISPRS Arch.*, vol. 38, pp. 520–525, 2010.
[42] Y. Chen, J. Wang, J. Li, C. Lu, Z. Luo, H. Xue, and C. Wang, "LiDAR-video dataset: Learning driving policies effectively," in *Proc. Conf. Comput. Vis. Pattern Recognit.*, 2018, pp. 5870–5878.

Yiping Chen (S'07–M'11) received the Ph.D. degree in information and communications engineering from the National University of Defense Technology, Changsha, China, in 2011.

She is an Assistant Professor with the National University of Defense Technology, and a Postdoctoral Fellow with the Fujian Key Laboratory of Sensing and Computing for Smart Cities and the School of Informatics, Xiamen University, Xiamen, China. From 2007 to 2011, she was an Assistant Researcher with the Chinese University of Hong Kong, Hong Kong. Her current research interests include image processing, mobile laser scanning data analysis, and three-dimensional point cloud object detection.

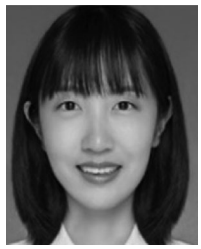

Shiqian Wang received the B.Sc. degree in geomatics from Wuhan University, Wuhan, China, in 2012, and the M.Sc. degree in geomatics from the University of Waterloo, Waterloo, ON, Canada, in 2016. She is currently working toward the Ph.D. degree in geography with Florida State University, Tallahassee, FL, USA.

Her research interests include image processing, point cloud processing, and remote sensing in forestry studies.

Jonathan Li (M'00–SM'11) received the Ph.D. degree in geomatics engineering from the University of Cape Town, Cape Town, South Africa.

He is currently a Professor with the Department of Geography and Environmental Management and Department of Systems Design Engineering, University of Waterloo, Waterloo, ON, Canada, and is also with the Fujian Key Laboratory of Sensing and Computing for Smart Cities, School of Informatics, Xiamen University, Xiamen, China. His research has been funded by the Natural Sciences and Engineering Research Council (NSERC) of Canada, Canada Foundation for Innovation (CFI), Agriculture and Agri-Food Canada (AAFC), Canadian Space Agency (CSA), Ministry of Transportation of Ontario (MTO), and industries. He has coauthored more than 400 publications, including more than 160 refereed journal papers. He has supervised more than ten Ph.D. and 50 master.s students to completion. His main research interests include light detection and ranging and synthetic aperture radar data processing, machine learning, and remote sensing applications.

He is currently serving as the Associate Editor for the IEEE JOURNAL OF SELECTED TOPICS IN APPLIED EARTH OBSERVATIONS AND REMOTE SENSING, IEEE TRANSACTIONS ON INTELLIGENT TRANSPORTATION SYSTEMS, and *Canadian Journal of Remote Sensing.*

Lingfei Ma (S'18) received the B.Sc. and M.Sc. degrees in geomatics in 2015 and 2017, respectively, from the University of Waterloo, Waterloo, ON, Canada, where he is currently working toward the Ph.D. degree in photogrammetry and remote sensing with the Mobile Sensing and Geodata Science Lab, Department of Geography and Environmental Management.

His research interests include autonomous driving, mobile laser scanning, intelligent processing of point clouds, three-dimensional scene modeling, and machine learning.

Rongren Wu received the B.Sc. degree in applied physics from Fuzhou University, Fuzhou, China, in 2016. He is currently working toward the M.Sc. degree in signal and information processing with the Fujian Key Laboratory of Sensing and Computing for Smart Cities and the School of Informatics, Xiamen University, Xiamen, China.

His research interests include intelligent processing of point clouds including point cloud segmentation, detection, extraction, three-dimensional computer vision, and machine learning.

Zhipeng Luo (S'19) received the B.Sc. degree in mathematics from the School of Mathematics and Statistics, Minnan Normal University, Zhangzhou, China, and the M.Sc. degree in computer science from the College of Mathematics and Computer Science, Fuzhou University, Fuzhou, China. He is currently working toward the Ph.D. degree in photogrammetry and remote sensing with the Fujian Key Laboratory of Sensing and Computing for Smart Cities and the School of Informatics, Xiamen University, Xiamen, China.

His research interests include autonomous driving, mobile laser scanning, intelligent processing of point clouds, three-dimensional computer vision, and machine learning.

Cheng Wang (M'07–SM'16) received the Ph.D. degree in signal and information processing from the National University of Defense Technology, Changsha, China, in 2002.

He is currently a Professor with the School of Informatics, and the Executive Director with the Fujian Key Laboratory of Sensing and Computing for Smart Cities, Xiamen University, Xiamen, China. He has coauthored more than 150 papers in referred journals and top conferences including IEEE TRANSACTIONS ON GEOSCIENCE AND REMOTE SENSING, PR, IEEE TRANSACTIONS ON INTELLIGENT TRANSPORTATION SYSTEMS, IEEE Conference on Computer Vision and Pattern Recognition, Association for the Advancement of Artificial Intelligence (AAAI), and *International Society for Photogrammetry and Remote Sensing (ISPRS) Journal of Photogrammetry and Remote Sensing*. His current research interests include point cloud analysis, multisensor fusion, mobile mapping, and geospatial big data.

Prof. Wang is a Fellow of the Institution of Engineering and Technology. He is also the Chair of the Working Group I/6 on Multi-Sensor Integration and Fusion of the International Society of Remote Sensing.